ISSN 1029-9599, Physical Mesomechanics, 2024, Vol. 27, No. 1, pp. 57–68. © Pleiades Publishing, Ltd., 2024.
Russian Text © The Author(s), 2023, published in Fizicheskaya Mezomekhanika, 2023, Vol. 26, No. 5, pp. 80–92.

Combination Effect of Transition Metal Impurities on Oxygen Vacancy Formation Energetics in TiO_2

A. V. Bakulin[1]*, L. S. Chumakova[1], S. O. Kasparyan[1,2], and S. E. Kulkova[1,2]

[1] *Institute of Strength Physics and Materials Science, Siberian Branch, Russian Academy of Sciences, Tomsk, 634055 Russia*

[2] *National Research Tomsk State University, Tomsk, 634050 Russia*

** e-mail: bakulin@ispms.ru*

Received January 27, 2023; revised April 7, 2023; accepted April 8, 2023

Abstract—The combination effect of substitutional impurities of group IVB–VIB transition metals on the oxygen vacancy formation energy in rutile titania was studied by the projector augmented wave method within density functional theory. The pair interaction energy of impurity atoms was estimated depending on the interatomic distance. It was shown that the interaction in the Zr + Zr, Hf + Hf and Nb + Ta pairs leads to the energy preference of their orientation along the ⟨100⟩ direction at a distance of the lattice parameter *a*. The Mo + Mo and Nb + Mo pairs prefer to orient along the [001] direction at a distance of the lattice parameter *c*. If the impurity atoms are farther than the third neighbors, then their interaction can be neglected. It was found that the change in the oxygen vacancy formation energy due to doping with several impurities can be estimated as the sum of the energy changes due to single impurity divided by a coefficient whose value depends on the mutual arrangement of the impurity atoms.

Keywords: TiO_2 oxide, doping, oxygen vacancy, impurity combination, density functional theory

DOI: 10.1134/S1029959924010065

1. INTRODUCTION

It is a common knowledge that doping and surface modification of TiAl-based alloys makes them attractive for use in aircraft engines, as components of gas turbines operating at temperatures up to 800°C, and in other fields [1–3]. An insufficient resistance of TiAl to oxidation is one of the key factors that reduces the service life and limits the operating temperature of the alloy parts [3–6]. It was experimentally found that the addition of a third component, such as Nb, Mo, W, or Re, improved the oxidation resistance of the TiAl alloy [7–11], while Mn and Cu worsened it [10–12]. Since experimental results are sensitive to many factors, such as temperature, partial pressure of oxygen, specimen purity, etc., the experiments often lead to contradictory conclusions. For example, such alloying elements as Cr, Ag, Hf, and Ta can be useful or undesirable from the corrosion resistance standpoint [9, 10, 13, 14]. The positive effect of the alloying elements on the oxidation resistance of TiAl alloy was explained by various factors: slowed diffusion of O in TiO_2 [14, 15], decreased solubility of Al in TiO_2 [11, 16], formation of a barrier layer on the surface or at the interface [14, 17], suppressed internal oxidation in the alloy [14, 18], and others. However, none of the proposed mechanisms is universal, and it is quite difficult to experimentally determine the key factors influencing the oxidation resistance of titanium alloys. Although the found mechanisms allow a specific selection of alloying elements, the selection criteria are vague due to the lack of the direct relation to fundamental parameters. Therefore, theoretical studies of physicochemical and mechanical properties of titanium aluminides remain relevant.

Currently, there are a large number of theoretical works devoted to the effect of impurities on the oxidation resistance of TiAl-based alloys. For example, the adsorption of oxygen on undoped and doped low-index TiAl alloy surfaces was studied in [19–25]. It was shown that, regardless of the surface orientation, oxygen was mainly adsorbed in titanium-rich positions, which favored the formation of TiO_2. With increasing oxygen concentration, O–Ti interactions compete with O–Al ones. Adhesive properties at the oxide–TiAl interface, as well as the influence of impurities and intermediate metal layers on its strength

characteristics, were studied in [26–32]. It was shown [26] that the addition of Nb caused oxygen atoms to displace from the oxide region to the alloy with the formation of O–Al bonds. This was taken as a proof of an increased interaction of oxygen with aluminum, responsible for the improvement of oxygen resistance of the alloy. The authors of [26–29] suggested that adhesion at an ideal interface was governed by the formation of O–Al bonds, while the authors of [30, 31] thought that the O–Ti interaction was the key factor. In [32], it was found that intermediate metal layers formed during segregation of the alloying element decreased adhesion, which however was quite high at the metal–oxide interface. Experimental works [33, 34 and references therein] revealed an increase in the oxidation resistance of TiAl alloy due to the formation of the Ti_5Si_3 phase at the interface. The diffusion coefficient of oxygen in Ti_5Si_3 was first calculated by theoretical methods in [35]. It was shown that this compound slowed down the diffusion of oxygen to rates characteristic of protective oxides such as Al_2O_3 or SiO_2. However, the authors of [36] pointed to the negative effect of the brittle Ti_5Si_3 phase at the interface. The influence of transition metal impurities on the energy of formation of Al_2O_3 and TiO_2 oxides, as well as the energy of formation of oxygen vacancies in the latter, was studied in [37]. It was discovered that Zr, Nb, Mo, Hf, Ta, W and Re impurities reduced the stability of Al_2O_3 as compared to that of TiO_2. Moreover, these impurities increased the oxygen vacancy formation energy in TiO_2. Based on these effects, we can conclude that these impurities have a positive influence on the oxidation resistance of TiAl alloy.

The theoretical works noted above allowed significant advances in the understanding of fundamental principles of TiAl oxidation. However, the question of the influence of impurities on the oxygen vacancy formation in TiO_2 remains open since only one configuration of the impurity-vacancy complex was studied [37]. It is known that impurities can suppress or, on the contrary, stimulate the formation of oxygen vacancies close and far from them. For example, the effect of impurities on oxygen sorption extends up to the fourth coordination sphere [38]. Though multicomponent TiAl-based alloys are studied experimentally, their theoretical investigation remains difficult and requires large computational resources. The influence of two or more impurity atoms on the oxygen vacancy formation in oxides has not been studied by theoretical methods. Thus, the aim of this work is to study the combination effect of group IVB–VIB impurities on oxygen vacancy formation energetics in rutile TiO_2.

2. CALCULATION PROCEDURE

The atomic and electronic structures of ideal and defective titania with a rutile structure were calculated using the projector augmented wave (PAW) method in a plane-wave basis [39, 40] using the generalized gradient approximation for the Perdew–Burke–Ernzerhof (GGA–PBE) exchange-correlation functional [41]. The maximum energy of plane waves in the basis set was 400 eV. The TiO_2 lattice parameters calculated in this work ($a = 0.4611$ nm, $c = 0.2956$ nm) differ from the experimental ones ($a = 0.4594$ nm, $c = 0.2959$ nm [42]) by less than 0.4%. The used supercell contained 216 atoms and measured $3 \times 3 \times 4$ to exclude the interaction between defects from the adjacent cells. Relaxation of the atomic structure, including optimization of atom positions, cell shape and volume, was implemented by the conjugate gradient method. The convergence criterion with respect to forces acting on atoms was 0.001 eV/nm. Self-consistency of the electronic subsystem was calculated accurate to 10^{-4} eV.

Since the formation energy of an O vacancy (V_O) depends on the chemical potential of oxygen, which is difficult to assess, it is more convenient to calculate the doping-induced change in this energy:

$$\Delta E_f = E_f^{dop} - E_f^{id} = E(TiO_2, V_O, X_{Ti}) - E(TiO_2, V_O) - E(TiO_2, X_{Ti}) + E(TiO_2), \quad (1)$$

where E_f^{dop} and E_f^{id} are the oxygen vacancy formation energies in the doped and undoped TiO_2; $E(TiO_2, V_O)$, $E(TiO_2, X_{Ti})$, and $E(TiO_2, V_O, X_{Ti})$ are the total energies of an oxide supercell containing an oxygen vacancy, substitutional impurity, and both defects; $E(TiO_2)$ is the total energy of the defect-free oxide. A positive (negative) value of ΔE_f means that the impurity increases (decreases) the formation energy of oxygen vacancies, i.e. contributes to a decrease (increase) in their equilibrium concentration.

The pair interaction energy of impurity atoms is calculated by the formula

$$\Delta E_{int} = E(TiO_2, X_{Ti}, Y_{Ti}) - E(TiO_2, X_{Ti}) - E(TiO_2, Y_{Ti}) + E(TiO_2), \quad (2)$$

where $E(TiO_2, X_{Ti})$, $E(TiO_2, Y_{Ti})$, and $E(TiO_2, X_{Ti}, Y_{Ti})$ are the total energies of the oxide with one (X or Y) and two impurity atoms in the Ti sublattice. A positive value of ΔE_{int} corresponds to repulsion between impurity atoms; a negative value, to attraction.

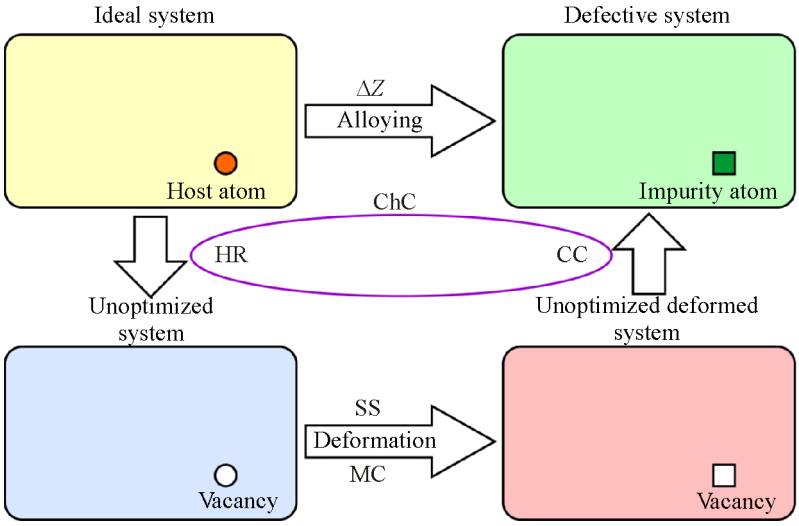

Fig. 1. Schematic of the method of decomposing the doping-induced change in the physical quantity ΔZ into contributions (for explanation see the text) (color online).

According to the method proposed in [43], if impurities are substitutional, the change in the physical quantity Z presents the sum of the three contributions: the host removal (HR), substitutional structure (SS) and chemical + compressed impurity (CC) mechanisms:

$$\Delta Z = \mathrm{HR} + \mathrm{SS} + \mathrm{CC}. \quad (3)$$

These contributions are schematized in Fig. 1. For ease of analysis, the first contribution responsible for breaking of old bonds and the third one associated with the formation of new bonds can be combined into the chemical contribution (ChC). The remaining SS contribution is associated only with structural deformation induced by impurity and can be regarded as the mechanical contribution (MC).

3. RESULTS AND DISCUSSION

3.1. Influence of Single Impurity on Oxygen Vacancy Formation Energy

As mentioned above, the energetics of formation of oxygen vacancies in doped titania was studied in [37]. It was shown that V and Cr impurities reduced the O vacancy formation energy, while metals isoelectronic with them and titanium, on the contrary, increased it. Investigation was given only to one position of the first-neighbor oxygen vacancies, without modeling vacancies father from impurity atoms. As will be shown below, consideration for second- or third-neighbor impurities can lead to different conclusions.

Since the rutile lattice has a tetragonal structure, coordination polyhedra are circumscribed by ellipsoids rather than coordination spheres. Let us number the coordination polyhedra in increasing order of the largest semi-axis of the circumellipsoid. Figure 2 shows the first four coordination polyhedra with oxygen atoms at the vertices and a titanium atom at the center. Oxygen atoms occupy 4f Wyckoff positions, which are displaced in the ⟨110⟩ direction from the highly symmetrical configuration. Therefore, several positions differently spaced from the central titanium atom can be distinguished for them in each coordination polyhedron. Distances between oxygen atoms and the central titanium atom in these polyhedra are cited in Table 1. For example, each titanium atom in the first coordination polyhedron is coordinated by six oxygen atoms, four of which ($1nn_1$) are located closer to the titanium atom, and two ($1nn_2$) are farther (Fig. 2a and Table 1). The designation nn comes from the nearest neighbor term. The same is true for the second neighbors: four oxygen atoms ($2nn_1$) are located slightly closer than the other four ($2nn_2$) (Fig. 2b). Since the oxygen atoms of the third coordination polyhedron form a straight quadrangular prism with a titanium atom at its geometric center (Fig. 2c), all $Ti–O_{3nn}$ interatomic distances are the same. Finally, in the fourth coordination polyhedron, oxygen atoms (4nn) form a complex polyhedron and can be divided into three groups, as shown in Fig. 2d.

Figure 3 illustrates the change in the formation energy of an oxygen vacancy depending on its position relative to the impurity atom. It can be seen that almost all the impurities increase the energy of formation of both oxygen vacancies in the first coordination polyhedron, which is consistent with the early

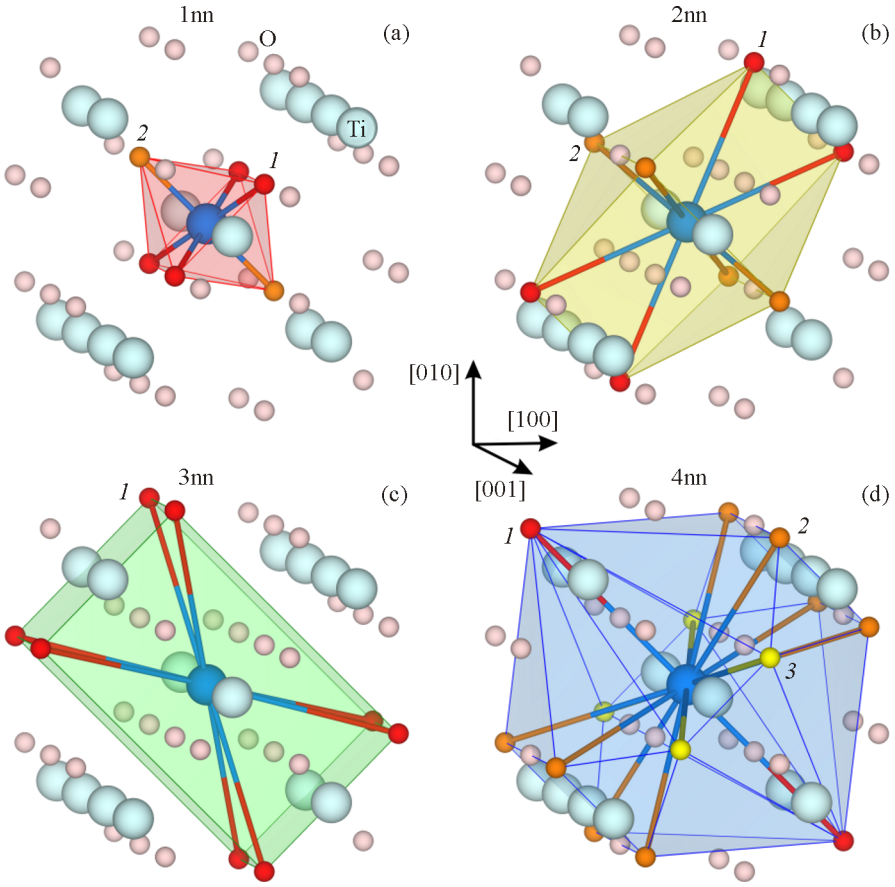

Fig. 2. First four coordination polyhedra of oxygen atoms relative to the given titanium atom. Digits indicate the group of oxygen atoms belonging to the same coordination polyhedron but differently spaced from the given titanium atom (color online).

results [37]. However, the situation is more complex for more distant vacancies. For example, Zr, Hf, and Mo reduce the energy of formation of the second- and third-neighbor oxygen vacancies, while the other metals, on the contrary, increase it.

From Fig. 3 it is also clear that the E_f increase occurs by different mechanisms. Thus, when doping with group IVB metals, the energy of formation of O vacancies in almost all positions changes due to the mechanical contribution (Figs. 3a, 3d). This is explained by the fact that these metals are isoelectronic with titanium, and the size factor plays the key role in changing E_f. The covalent radii of Zr and Hf are equal to 0.175 nm [44], being most different from the Ti radius (0.160 nm). The chemical contribution, i.e. the O_V–X_{Ti} interaction, dominates only for the $1nn_1$ vacancy, closest to the impurity atom. As for group VB impurities, the absolute values of ChC and MC generally increase, through the key contribution is chemical (Figs. 3b, 3e). The decreasing role of the size effect is associated with similar covalent radii of Ti, Nb, and Ta (0.160, 0.164, and 0.170 nm [44]), and the increasing role of the chemical interaction is explained by a higher occupancy of the *d* shell of the VB group impurity atom. When doping with VIB impurities, the covalent radii of Mo (0.154 nm) and W (0.162 nm) are similar to the Ti radius, and therefore the E_f change is mainly determined by the chemical contribution (Figs. 3c, 3f). When a vacancy is located at the vertex of the fourth coordination

Table 1. Distances *d* between oxygen and titanium atoms and the number of oxygen atoms *N* at the vertices of the first four titanium coordination polyhedra

Coordination polyhedron	O atom group	*N*	*d*(Ti–O), nm
1nn	1	4	0.197
	2	2	0.201
2nn	1	4	0.354
	2	4	0.358
3nn	1	8	0.414
4nn	1	2	0.458
	2	8	0.462
	3	4	0.464

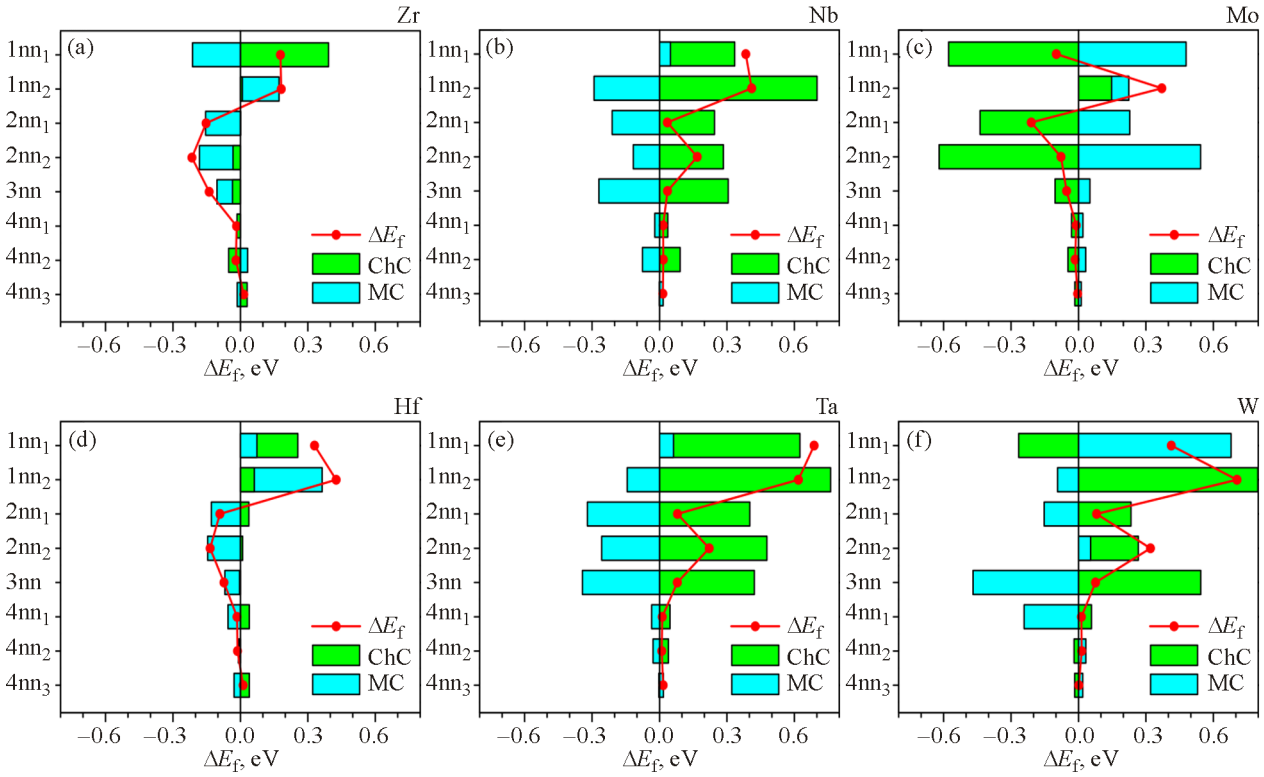

Fig. 3. Change of the oxygen vacancy formation energy in TiO_2 due to doping with Zr (a), Nb (b), Mo (c), Hf (d), Ta (e) and W (f) impurities, as well as chemical and mechanical contributions to ΔE_f (color online).

polyhedron, the absolute values of ΔE_f do not exceed 0.02 eV. Thus, the impurity is assumed to affect the vacancy formation energy only within the first three coordination polyhedra.

3.2. Interaction between Impurity Atoms

Before proceeding to the combination effect of impurities on the oxygen vacancy formation energy in TiO_2, it is necessary to determine energetically preferred structural configurations. For this purpose, the interaction energy between impurity atoms is calculated depending on the distance between them. Titanium atoms located at the vertices of the first six coordination polyhedra are shown in Fig. 4. Since titanium atoms are arranged in a body-centered tetragonal lattice with the ratio $c/a < \sqrt{2/3}$, the nearest neighbors are not eight atoms located in the cell vertices, as with a body-centered cubic structure, but two atoms of the neighboring cells in the direction ⟨001⟩ (Fig. 4a). Coordination polyhedra with titanium atoms at the vertices and at the center will be denoted by capital NN. Figure 4b shows that the mentioned eight atoms correspond to the second coordination polyhedron. The third coordination polyhedron contains four titanium atoms arranged in a square and located at the distance a from the given atom (Fig. 4c). The fourth coordination polyhedron includes two types of atoms: eight atoms at the distance equal to the diagonal of the lateral face of the rutile cell and eight atoms displaced from the given atom by $a/2$ and $3c/2$ (Fig. 4d). As can be seen from Fig. 4e, the fifth neighbors are two atoms located at the distance $2c$ from the given atom. Interestingly, the sixth neighbor titanium atoms are also arranged in a planar configuration (Fig. 4f), like the 3NN atoms. Structural parameters of the coordination polyhedra are given in Table 2.

The calculations show that 3NN is energetically the most preferred configuration for pairs of impurity atoms isoelectronic with titanium, i.e. for Zr and Hf (Figs. 5a, 5d). This suggests that the interacting impurity atoms tend to form atomic chains in the ⟨100⟩ direction. Group VB elements (Nb and Ta) have no tendency to form ordered structures in TiO_2 since $\Delta E_{int} \geq 0$ in the considered configurations (Figs. 5b, 5e). Nevertheless, the smallest ΔE_{int} also corresponds to the 3NN configuration. According to the calculations, Mo and W atoms are also prone to form chains, but in the [001] direction, since ΔE_{int} is the most negative value in the 1NN configuration (Figs. 5c, 5f).

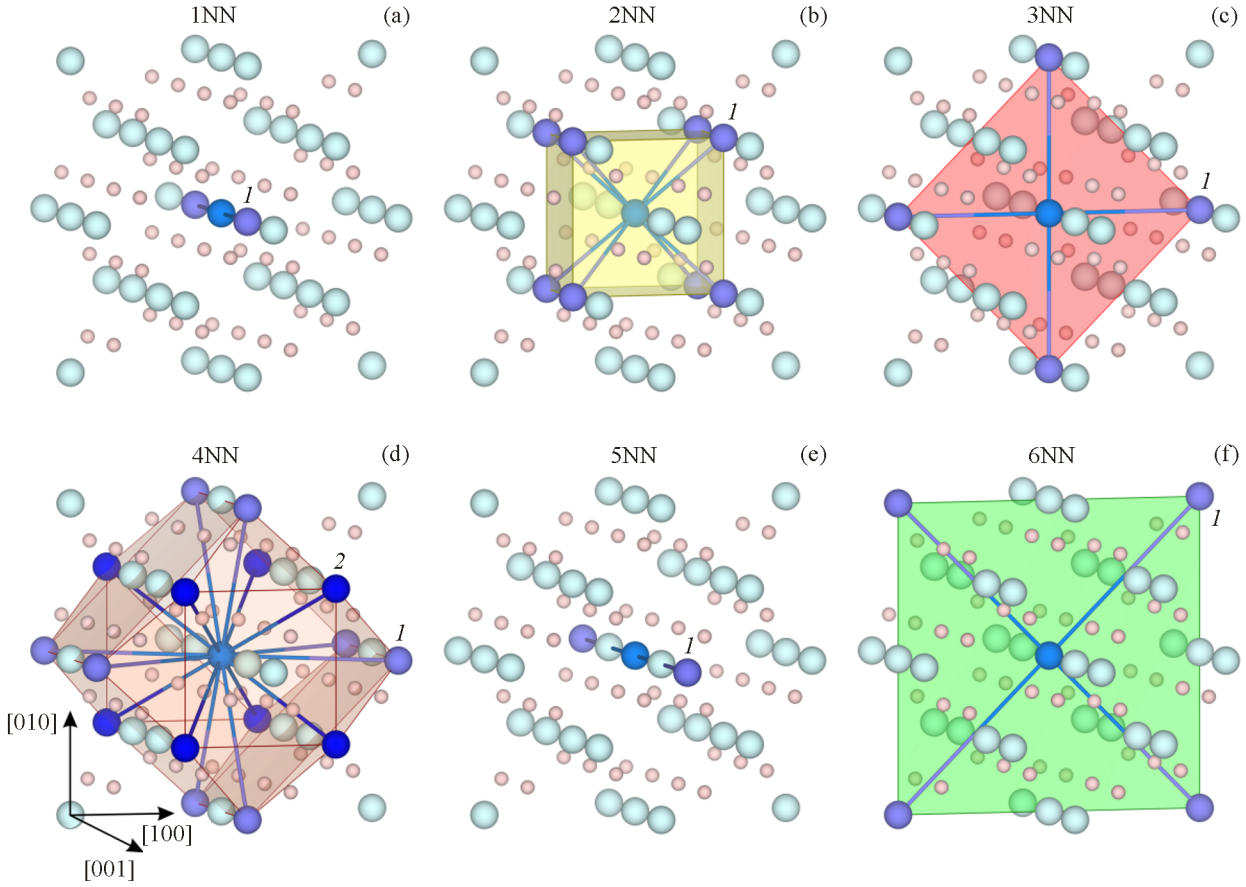

Fig. 4. First six coordination polyhedra of titanium relative to the given titanium atom. Digits indicate the group of titanium atoms belonging to the same coordination polyhedron but differently spaced from the given titanium atom (color online).

This tendency is much more pronounced for Mo ($\Delta E_{int} = -0.93$ eV) than for W ($\Delta E_{int} = -0.02$ eV). The interaction of the Nb and Mo impurity atoms stabilizes the 1NN structure (Fig. 5g). Though the Nb–Nb and Ta–Ta interactions result in no stable configurations, their combination (Nb + Ta) energetically prefers to form in the 3NN configuration (Fig. 5h). When doping the oxide with Nb and W, no stable configurations are formed (Fig. 5i).

3.3. Influence of Two Impurity Atoms on Oxygen Vacancy Formation Energy

In the presence of two impurity atoms, an oxygen vacancy can form in two positions: (1) near (up to

Table 2. Distances d between titanium atoms in terms of lattice parameters, their values and the number of titanium atoms N at the vertices of the first six titanium coordination polyhedra

Coordination polyhedron	Ti atom group	N	d(Ti–Ti)	d(Ti–Ti), nm
1NN	1	2	c	0.2956
2NN	1	8	$0.5\sqrt{2a^2 + c^2}$	0.3579
3NN	1	4	a	0.4610
4NN	1	8	$\sqrt{a^2 + c^2}$	0.5476
	2	8	$0.5\sqrt{2a^2 + 9c^2}$	0.5503
5NN	1	2	$2c$	0.5912
6NN	1	4	$a\sqrt{2}$	0.6520

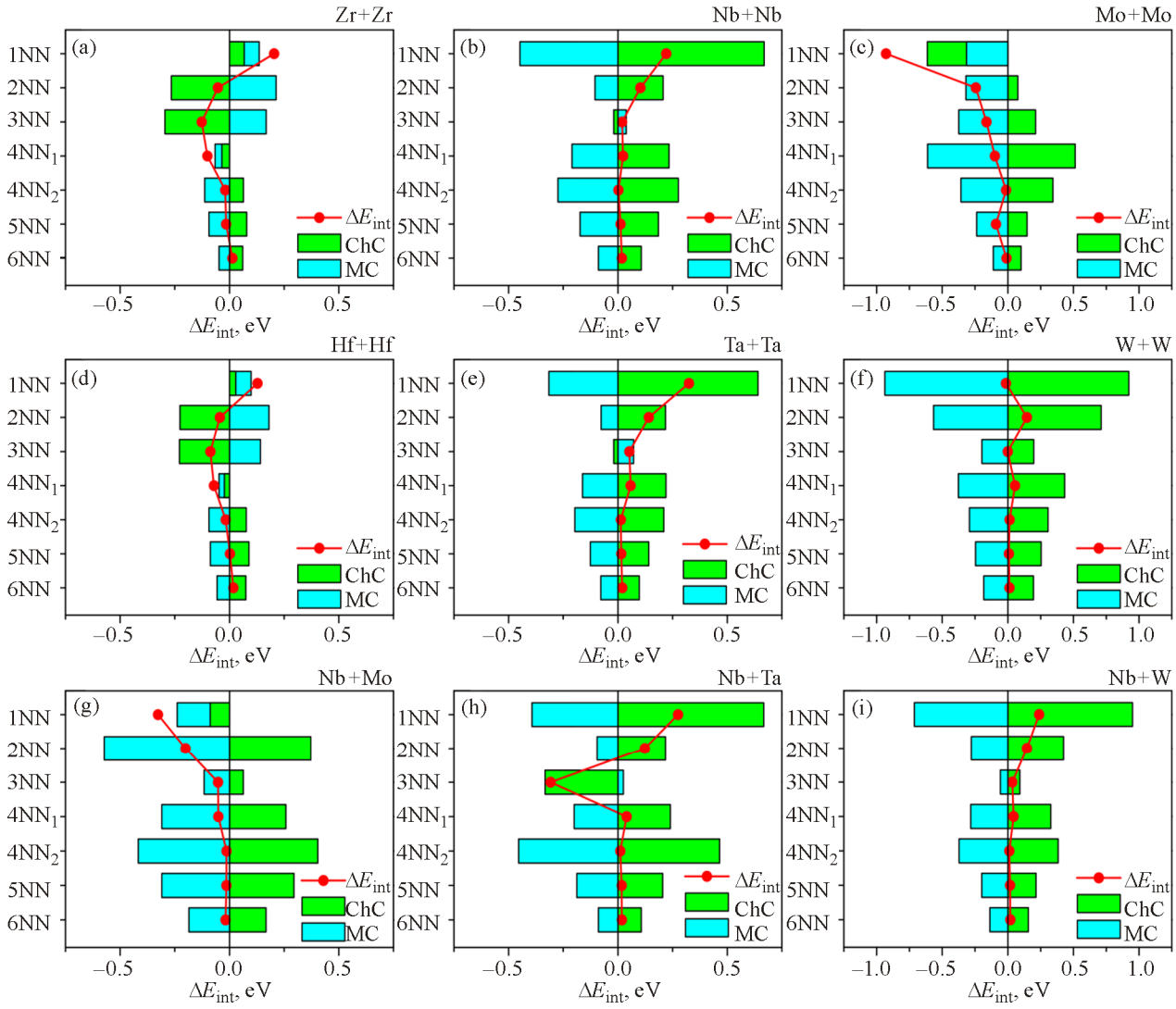

Fig. 5. Interaction energy between two impurity atoms in TiO_2, as well as chemical and mechanical contributions (color online).

3nn inclusive) both impurity atoms, and (2) near one of the impurity atoms. In the first case, in the 3NN configuration of impurity atoms (Fig. 4c), a vacancy can be located in position $1nn_2$ relative to one atom and position $2nn_1$ relative to the other (c1) or in $1nn_1$ and 3nn (c2). In the second case, a vacancy can be in positions $1nn_1$, $1nn_2$, $2nn_1$, $2nn_2$ or 3nn relative to one of the impurity atoms and more distant from the other. If impurity atoms are arranged in a 1NN structure (Fig. 4a), a vacancy, in the first case, can occupy position $1nn_1$ (c1) or 3nn (c3) relative to both impurity atoms as well as positions $1nn_2$ and $2nn_2$ (c2). In the second case, a vacancy has the same positions as in the 1NN configuration, except for position $1nn_2$.

Changes in the formation energy of oxygen vacancies ($\Delta E_f(X_{Ti}+Y_{Ti})$) in the mentioned positions are shown in Fig. 6a. It also interesting to compare the effect of double impurity with the data obtained for the respective single impurities, i.e. the additive effect $\Delta E_f(X_{Ti})+\Delta E_f(Y_{Ti})$, which is shown by blue squares in Fig. 6a. For convenience, the difference between these changes will be denoted as ε:

$$\varepsilon = \Delta E_f(X_{Ti}) + \Delta E_f(Y_{Ti}) - \Delta E_f(X_{Ti}+Y_{Ti}). \quad (4)$$

It was earlier found [38] for Ti_3Al alloy that the change in oxygen absorption energy near two impurity atoms can be accurately estimated as the sum of changes caused by the single impurities ($\varepsilon < 0.11$ eV or <9% of the true value). However, judging from Fig. 6a, this does not hold for the oxygen vacancy formation energy in the oxide: the estimated values are significantly (1.5–2 times) higher than the true

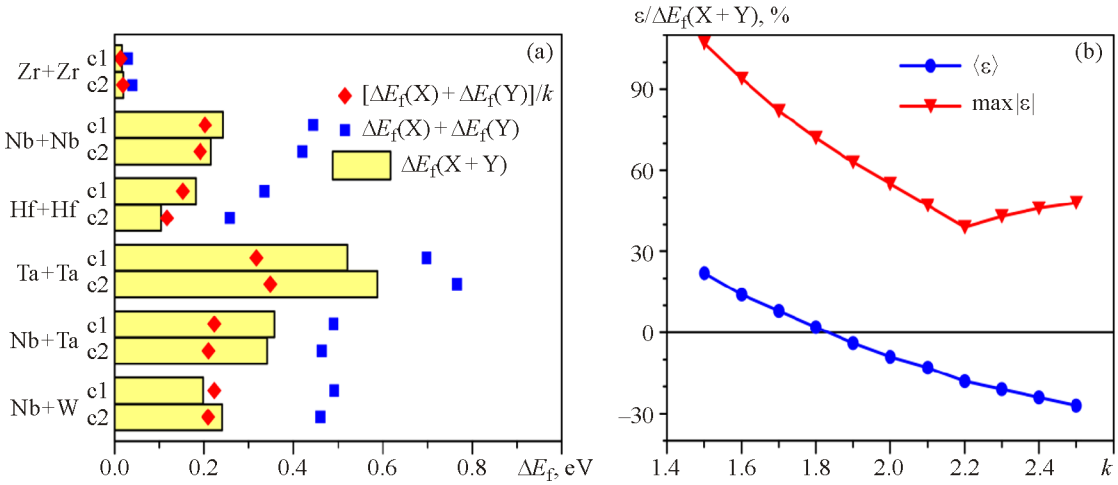

Fig. 6. Change of the oxygen vacancy formation energy in positions c1 and c2 near two impurity atoms in the 3NN configuration (a), dependence of the average and maximum absolute values of the parameter ε on the weakening coefficient k (b) (color online).

ones. This may be due to the fact that the oxide (insulator) is capable of a long-range contribution to the interaction energy due to weaker shielding compared to the alloy (conductor). Assuming that the interaction between impurity atoms weakens the influence of each impurity, the weakening coefficient k can be empirically chosen. Figure 6b plots the ratios of the average and maximum absolute values of ε to the true $\Delta E_f(X_{Ti}+Y_{Ti})$ as a function of the parameter k. Averaging is carried out over all impurity pairs with the preferred 3NN configuration. It can be seen that, at $k=2.2$, the maximum deviation is 39%, which is the absolute minimum for this model. The maximum deviation is obtained for the Ta+Ta and Nb+Ta pairs with c1 and c2 vacancies, which corresponds to 0.22 and 0.13 eV. At $k=2.2$, the change in the oxygen vacancy formation energy is underestimated, on the average, by 18% or 0.06 eV. In the undoped oxide, the oxygen vacancy formation energy is 4.3 eV [37]. Thus, the maximum deviation of the adjusted estimated energy of oxygen vacancy formation from its true value does not exceed ~5.5%. The ΔE_f values estimated with consideration for the weakening coefficient are shown in Fig. 6a by red rhombs.

The simple additive model of the influence of impurities is also inapplicable to the Mo+Mo, W+W and Nb+Mo pairs with the preferred 1NN configuration (Fig. 7a). The weakening parameter is adjusted by minimizing the maximum deviation, resulting in the value $k=2.7$ (Fig. 7b). In this case, the maximum deviation is 23%, which corresponds to –0.007, –0.017, and 0.002 eV for the Mo+Mo, W+W and Nb+Mo pairs with a c3 vacancy. The maximum absolute deviation is 0.08–0.09 eV (18–21%), which is

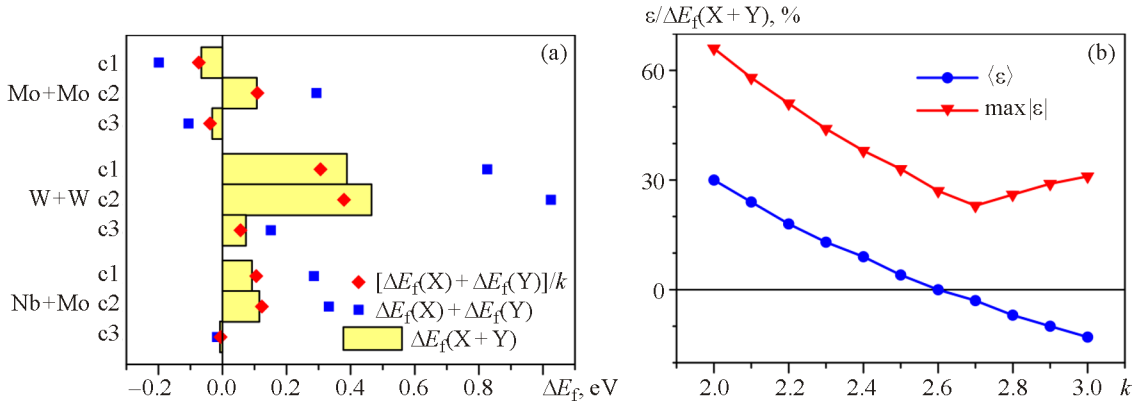

Fig. 7. Change of the oxygen vacancy formation energy in positions c1, c2, and c3 near two impurity atoms in the 1NN configuration (a), dependence of the average and maximum absolute values of the parameter ε on the weakening coefficient k (b) (color online).

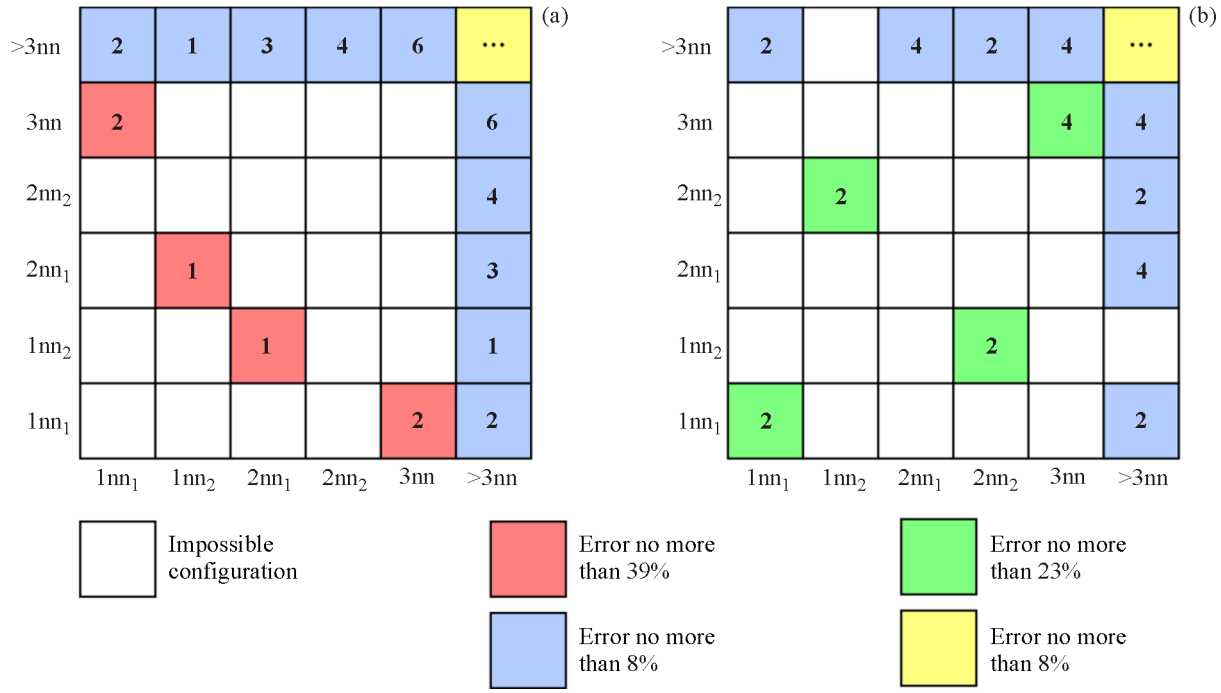

Fig. 8. Schematic representation of possible positions of an oxygen vacancy in TiO_2 relative to a pair of impurity atoms in the 3NN (a) and 1NN configurations (b). Digits in the squares indicate the number of configurations (color online).

obtained for the W + W pair with c1 and c2 vacancies. Thus, the error of the ΔE_f estimation for these impurity pairs is comparable to the calculation error of the interaction energy between impurity atoms.

If a vacancy is farther from the impurity atom than the third neighbors, the deviation of the estimated ΔE_f from the true values is small and does not exceed 8% in the 3NN and 1NN configurations of impurity atoms. The crystal volume can be divided into several regions depending on the vacancy position relative to a pair of impurity atoms. For illustration, these regions are marked with different squares in Fig. 8: white squares correspond to impossible combinations of V_O with X_{Ti} and Y_{Ti}; red and green, to case 1; blue, to case 2; yellow, to vacancy positions far from both impurities.

In conclusion, it may be said that the oxygen diffusion coefficient in doped TiO_2 can be estimated based on the average energies of oxygen vacancy formation and migration along each of the three possible paths (see, for example, [45, 46]). The first characteristic should be calculated with consideration for the number of positions near both impurities, near one of them, and far from both (digits in Fig. 8). To find the second characteristic, it suffices to know the energies of oxygen vacancy migration between the red (green) and blue regions or within them. As was shown in [47] for hydrogen, the change in the migration energy along other paths can be neglected.

4. CONCLUSIONS

The influence of two substitutional atoms (Zr, Nb, Mo, Hf, Ta, W) on the oxygen vacancy formation energy in rutile TiO_2 depending on their relative position was studied by the projector augmented wave method. It was shown that the substitution of a Ti atom increased the oxygen vacancy formation energy by 0.1–0.7 eV for the first-neighbor vacancies relative to the impurity atom. The mechanism of this effect depends on the group of the impurity element in the periodic table. If a vacancy was located at the vertex of the second or third coordination polyhedron, then only Zr, Hf and Mo impurities reduced E_f by 0.1–0.2 eV. In the case of the first two impurities, this was mainly due to the mechanical contribution. The replacement of a titanium atom with a larger one partially compensated for the lattice compression during vacancy formation. When doping with molybdenum, the E_f decrease was caused mainly by the chemical contribution, although there was no direct impurity–vacancy interaction. If the vacancy was farther than the third neighbors of the impurity atom, then the influence of the latter can be neglected, since

the absolute value of their interaction energy did not exceed 0.02 eV.

The interaction energy between two impurity atoms was estimated depending on their position. It was shown that the Zr–Zr, Hf–Hf and Nb–Ta interaction stabilized the 3NN configuration when the impurity atoms were the third neighbors of each other. The interaction energy in the Mo + Mo and Nb + Mo pairs reached its lowest value in the 1NN configuration. Change in the oxygen vacancy formation energy caused by the interaction with two impurity atoms can be estimated as the sum of the changes due to single impurities with consideration for the weakening coefficient. By minimizing the maximum deviation of the estimated ΔE_f from the true value, the weakening coefficient (2.2 and 2.7) was found for the 3NN and 1NN configurations of impurity atoms. In the first case, the estimation error did not exceed 0.09 eV (18%), while, in the second case, the maximum error was 0.22 eV (39%) for the Ta + Ta pair. Thus, this method makes it possible to estimate the influence of several impurities on the vacancy formation energy. This saves computing resources, by determining the most promising impurity combinations for accurate calculations.

FINDING

The work was granted by the Russian Science Foundation (project No. 21-73-00243). Numerical calculations were carried out on the SKIF Cyberia supercomputer at Tomsk State University.

CONFLICT OF INTEREST

The authors of this work declare that they have no conflicts of interest.

REFERENCES

1. Clemens, H. and Kestler, H., Processing and Applications of Intermetallic γ-TiAl-Based Alloys, *Adv. Eng. Mater*., 2000, vol. 2, pp. 551–570. https://doi.org/10.1002/1527-2648(200009)2:9<551::AID-ADEM551>3.0.CO;2-U
2. Appel, F., Paul, J.D.H., and Oehring, M., *Gamma Titanium Aluminide Alloys*, Weinheim: Wiley-VCH, 2011.
3. Li, Z. and Gao, W., High Temperature Corrosion of Intermetallics. Chapter 1, in *Intermetallics Research Progress*, Berdovsky, Y.N., Ed., New York: Nova Sci. Publ., 2008, pp. 1–64.
4. Umakoshi, Y., Yamaguchi, M., Sakagami, T., and Yamane, T., Oxidation Resistance of Intermetallic Compounds Al_3Ti and TiAl, *J. Mater. Sci*., 1989, vol. 24, pp. 1599–1603. https://doi.org/10.1007/BF01105677
5. Taniguchi, S., Shibata, T., and Itoh, S., Oxidation Behavior of TiAl at High Temperature in Purified Oxygen, *Mater. Trans. JIM*, 1991, vol. 32, no. 2, pp. 151–156. https://doi.org/10.2320/matertrans1989.32.151
6. Maurice, V., Despert, G., Zanna, S., Josso, P., Bacos, M.P., and Marcus, P., The Growth of Protective Ultra-Thin Alumina Layers on γ-TiAl(111) Intermetallic Single-Crystal Surfaces, *Surf. Sci*., 2005, vol. 596, pp. 61–73. https://doi.org/10.1016/j.susc.2005.09.011
7. Shida, Y. and Anada, H., Role of W, Mo, Nb and Si on Oxidation of TiAl in Air at High Temperatures, *Mater. Trans. JIM*, 1994, vol. 35, pp. 623–631. https://doi.org/10.2320/matertrans1989.35.623
8. Nickel, H., Zheng, N., Elschner, A., and Quadakkers, W.J., The Oxidation Behaviour of Niobium Containing γ-TiAl Based Intermetallics in Air and Argon/Oxygen, *Microchim. Acta*, 1995, vol. 119, pp. 23–39. https://doi.org/10.1007/BF01244851
9. Haanappel, V.A.C., Sunderkötter, J.D., and Stroosnijder, M.F., The Isothermal and Cyclic High Temperature Oxidation Behaviour of Ti–48Al–2Mn–2Nb Compared with Ti–48Al–2Cr–2Nb and Ti–48Al–2Cr, *Intermetallics*, 1999, vol. 7, no. 5, pp. 529–541. https://doi.org/10.1016/S0966-9795(98)00076-4
10. Shida, Y. and Anada, H., The Effect of Various Ternary Additives on the Oxidation Behavior of TiAl in High-Temperature Air, *Oxid. Met*., 1996, vol. 45, no. 1/2, pp. 197–219. https://doi.org/10.1007/BF01046826
11. Perkins, R.A., Chiang, K.T., and Meier, G.H., Formation of Alumina on Ti–Al Alloy, *Scripta Metall*., 1987, vol. 21, pp. 1505–1510. https://doi.org/10.1016/0036-9748(87)90291-2
12. Shida, Y. and Anada, H., The Influence of Ternary Element Addition on The Oxidation Behaviour of TiAl Intermetallic Compound in High Temperature Air, *Corros. Sci*., 1993, vol. 35, pp. 945–953. https://doi.org/10.1016/0010-938X(93)90313-6
13. Wang, F., Tang, Z., and Wu, W., Effect of Chromium on the Oxidation Resistance of TiAl Intermetallics, *Oxid. Met*., 1997, vol. 48, no. 5/6, pp. 381–390. https://doi.org/10.1007/BF02153457
14. Taniguchi, S. and, Shibata, T., Influence of Additional Elements on the Oxidation Behaviour of TiAl, *Intermetallics*, 1996, vol. 4, pp. S85–S93. https://doi.org/10.1016/0966-9795(96)00017-9
15. Hauffe, K., The Mechanism of Oxidation of Metals and Alloys at High Temperatures, *Progr. Metal. Phys*., 1953, vol. 4, pp. 71–104. https://doi.org/10.1016/0502-8205(53)90015-X
16. Schmitz-Niederau, M. and Schütze, M., The Oxidation Behavior of Several Ti-Al Alloys at 900°C in Air, *Oxid. Met*., 1999, vol. 52, pp. 225–240. https://doi.org/10.1023/A:1018839511102

17. Kasahara, K., Hashimoto, K., Doi, H., and Tsujimoto, T., High Temperature Oxidation Behavior of TiAl-Base Alloys with Additions of Third Elements, *J. Jpn. Inst. Met*., 1990, vol. 54, pp. 948–954. https://doi.org/10.2320/jinstmet1952.54.8_948
18. Wagner, C., Reaktionstypen bei der Oxydation von Legierungen, *Z. Elektrochem*., 1959, vol. 63, pp. 772–782. https://doi.org/10.1002/bbpc.19590630713
19. Liu, S.Y., Shang, J.X., Wang, F.H., and Zhang, Y., Ab Initio Study of Surface Self-Segregation Effect on the Adsorption of Oxygen on the γ-TiAl(111) Surface, *Phys. Rev. B*, 2009, vol. 79, p. 075419. https://doi.org/10.1103/PhysRevB.79.075419
20. Li, H., Wang, S., and Ye, H., Initial Oxidation of γ-TiAl (111) Surface: Density-Functional Theory Study, *J. Mater. Sci. Technol*., 2009, vol. 25, no. 4, pp. 569–576. https://www.jmst.org/EN/Y2009/V25/I04/569
21. Song, Y., Dai, J.H., and Yang, R., Mechanism of Oxygen Adsorption on Surfaces of γ-TiAl, *Surf. Sci*., 2012, vol. 606, pp. 852–857. https://doi.org/10.1016/j.susc.2012.01.024
22. Wang, L., Shang, J.X., Wang, F.H., Chen, Y., and Zhang, Y., Oxygen Adsorption on γ-TiAl Surfaces and the Related Surface Phase Diagrams: A Density-Functional Theory Study, *Acta Mater*., 2013, vol. 61, pp. 1726–1738. https://doi.org/10.1016/j.actamat.2012.11.047
23. Kulkova, S.E., Bakulin, A.V., Hu, Q.M., and Yang, R., Adsorption and Diffusion of Oxygen on γ-TiAl(001) and (100) Surfaces, *Comput. Mater. Sci*., 2015, vol. 97, pp. 55–63. https://doi.org/10.1016/j.commatsci.2014.10.007
24. Bakulin, A.V., Kulkova, S.E., Hu, Q.M., and Yang, R., Theoretical Study of Oxygen Sorption and Diffusion in the Volume and on the Surface of a γ-TiAl Alloy, *JETP*, 2015, vol. 120, no. 2, pp. 257–367.
25. Kulkova, S.E., Bakulin, A.V., and Kulkov, S.S., Oxygen Adsorption on the Doped TiAl(100) Surface, *Comput. Mater. Sci*., 2019, vol. 170, p. 109136. https://doi.org/10.1016/j.commatsci.2019.109136
26. Song, Y., Xing, F.J., Dai, J.H., and Yang, R., First-Principles Study of Influence of Ti Vacancy and Nb Dopant on the Bonding of TiAl/TiO_2 Interface, *Intermetallics*, 2014, vol. 49, pp. 1–6. https://doi.org/10.1016/j.intermet.2014.01.001
27. Wang, B., Dai, J., Wu, X., Song, Y., and Yang, R., First-Principles Study of the Bonding Characteristics of TiAl(111)/Al_2O_3(0001) Interface, *Intermetallics*, 2015, vol. 60, pp. 58–65. https://doi.org/10.1016/j.intermet.2015.02.001
28. Dai, J.H., Song, Y., and Yang, R., Influence of Alloying Elements on Stability and Adhesion Ability of TiAl/TiO_2 Interface by First-Principles Calculations, *Intermetallics*, 2017, vol. 85, pp. 80–89. https://doi.org/10.1016/j.intermet.2017.02.007
29. Li, Y., Dai, J.H., and Song, Y., Enhancing Adhesion of Al_2O_3 Scale on Ti-Al Intermetallics by Alloying: A First Principles Study, *Comput. Mater. Sci*., 2020, vol. 181, p. 109756. https://doi.org/10.1016/j.commatsci.2020.109756
30. Bakulin, A.V., Kulkov, S.S., and Kulkova, S.E., Condensed State Adhesive Properties of the TiAl/Al_2O_3 Interface, *Russ. Phys. J.*, 2020, vol. 63, no. 5, pp. 713–720.
31. Bakulin, A.V., Kulkov, S.S., Kulkova, S.E., Hocker, S., and Schmauder, S., First Principles Study of Bonding Mechanisms at the TiAl/TiO_2 Interface, *Metals*, 2020, vol. 10, p. 1298. https://doi.org/10.3390/met10101298
32. Bakulin, A.V., Hocker, S., and Kulkova, S.E., Role of Intermediate Metal and Oxide Layers in Change of Adhesion Properties of TiAl/Al_2O_3 Interface, *Phys. Mesomech.*, 2021, vol. 24, no. 5, pp. 523–532. https://doi.org/10.1134/S1029959921050039
33. Li, X.Y., Taniguchi, S., Matsunaga, Y., Nakagawa, K., and Fujita, K., Influence of Siliconizing on the Oxidation Behavior of a γ-TiAl Based Alloy, *Intermetallics*, 2003, vol. 11, pp. 143–150. https://doi.org/10.1016/S0966-9795(02)00193-0
34. Huang, J., Zhao, F., Cui, X., Wang, J., and Xiong, T., Long-Term Oxidation Behavior of Silicon-Aluminizing Coating with an In-Situ Formed Ti_5Si_3 Diffusion Barrier on γ-TiAl Alloy, *Appl. Surf. Sci*., 2022, vol. 582, p. 152444. https://doi.org/10.1016/j.apsusc.2022.152444
35. Bakulin, A.V., Chumakova, L.S., and Kulkova, S.E., Oxygen Absorption and Diffusion in Ti_5Si_3, *Intermetallics*, 2022, vol. 146, p. 107587. https://doi.org/10.1016/j.intermet.2022.107587
36. Jiang, H.R., Wang, Z.L., Ma, W.S., Feng, X.R., Dong, Z.Q., Zhang, L., and Liu, Y., Effects of Nb and Si on High Temperature Oxidation of TiAl, *Trans. Nonferrous Met. Soc. China*, 2008, vol. 18, pp. 512–517. https://doi.org/10.1016/S1003-6326(08)60090-4
37. Ping, F.P., Hu, Q.M., Bakulin, A.V., Kulkova, S.E., and Yang, R., Alloying Effects on Properties of Al_2O_3 and TiO_2 in Connection with Oxidation Resistance of TiAl, *Intermetallics*, 2016, vol. 68, pp. 57–62. https://doi.org/10.1016/j.intermet.2015.09.005
38. Bakulin, A.V., Chumakova, L.S., Kasparyan, S.O., and Kulkova, S.E., Impurity Combination Effect on Oxygen Absorption in α_2-Ti_3Al, *Metals*, 2022, vol. 12, p. 650. https://doi.org/10.3390/met12040650
39. Blöchl, P.E., Projector Augmented-Wave Method, *Phys. Rev. B*, 1994, vol. 50, no. 24, pp. 17953–17979. https://doi.org/10.1103/PhysRevB.50.17953
40. Kresse, S. and Joubert, D., From Ultrasoft Pseudopotentials to the Projector Augmented-Wave Method, *Phys. Rev. B*, 1999, vol. 59, pp. 1758–1775. https://doi.org/10.1103/PhysRevB.59.1758

41. Perdew, J.P., Burke, K., and Ernzerhof, M., Generalized Gradient Approximation Made Simple, *Phys. Rev. Lett*., 1996, vol. 77, no. 18, pp. 3865–3868. https://doi.org/10.1103/PhysRevLett.77.3865
42. Abrahams, S.C. and Bernstein, J.L., Rutile: Normal Probability Plot Analysis and Accurate Measurement of Crystal Structure, *J. Chem. Phys.*, 1971, vol. 55, no. 7, pp. 3206–3211. https://doi.org/10.1063/1.1676569
43. Lozovoi, A.Y., Paxton, A.T., and Finnis, M.W., Structural and Chemical Embrittlement of Grain Boundaries by Impurities: A General Theory and First-Principles Calculations for Copper, *Phys. Rev. B*, 2006, vol. 74, p. 155416. https://doi.org/10.1103/PhysRevB.74.155416
44. Cordero, B., Gómez, V., Platero-Prats, A.E., Revès, M., Echeverría, J., Cremades, E., Barragán, F., and Alvarez, S., Covalent Radii Revisited, *Dalton Trans*., 2008, vol. 21, pp. 2832–2838. https://doi.org/10.1039/B801115J
45. Zhu, L., Hu, Q.M., Yang, R., and Ackland, G.J., Atomic-Scale Modeling of the Dynamics of Titanium Oxidation, *J. Phys. Chem. C*, 2012, vol. 116, pp. 24201–24205. https://doi.org/10.1021/jp309305n
46. Bakulin, A.V., Chumakova, L.S., and Kulkova, S.E., Study of the Diffusion Properties of Oxygen in TiO_2, *JETP*, 2021, vol. 133, no. 2, pp. 169–174.
47. Bakulin, A.V., Kulkov, A.S., and Kulkova, S.E., Impurity Influence on the Hydrogen Diffusivity in B_2-TiFe, Int. *J. Hydrogen Energy*, 2023, vol. 48, pp. 232–242. https://doi.org/10.1016/j.ijhydene.2022.09.206